Oil & Gas Science and Technology – Rev. IFP, Vol. 61 (2006), No. 6, pp. 765-771

DOI: 10.2516/ogst:2006015

Dossier
Deformation of Solid Polymers
Déformation des polymères solides

Cohesive Zone Description and Quantitative Analysis of Glassy Polymer Fracture

N. Saad[1], R. Estevez[1], C. Olagnon[1] and R. Séguéla[1, 2]

1 MATEIS INSA Lyon, 20, avenue A. Einstein, 69621 Villeurbanne Cedex - France
2 Laboratoire Structure et Propriétés de l'État Solide, Bât. C6, Université de Lille I, 59655 Villeneuve d'Asq Cedex - France
e-mail: nesrine.saad@insa-lyon.fr - rafael.estevez@insa-lyon.fr - christian.olagnon@insa-lyon.fr - roland.seguela@insa-lyon.fr

Résumé — Modélisation par zone cohésive et étude expérimentale de la rupture des polymères vitreux — Le craquelage est décrit à l'aide d'une zone cohésive qui prend en compte l'amorçage, l'élargissement des surfaces des craquelures jusqu'à la rupture des fibrilles qui correspond à la création d'une fissure localement. Une calibration des paramètres de la zone cohésive est présentée pour le PMMA (Polymethyl methacrylate). Nous montrons qu'il est nécessaire de décrire le craquelage à l'aide d'une zone cohésive viscoplastique pour rendre compte des effets de la vitesse de chargement sur la ténacité du matériau, qui dépend des conditions de sollicitation.

Abstract — Cohesive Zone Description and Quantitative Analysis of Glassy Polymer Fracture — *Crazing is described with a viscoplastic cohesive zone which accounts for its initiation for a critical stress state, the thickening of the craze surfaces up to the failure of the craze fibrils which corresponds to the nucleation of a crack locally. A calibration of the parameters of such a cohesive zone is presented for PMMA (Polymethyl methacrylate). The rate dependent formulation of the cohesive zone is shown necessary to capture the rate dependency of the glassy polymer toughness.*

INTRODUCTION

Failure of amorphous polymers in the glassy state results from the competition between shear yielding and crazing. When crazing is suppressed, as in compression, the bulk material shows a localised plastic deformation through shear bands related to the softening upon yielding followed by a progressive strain hardening as the deformation continues. Crazing involves also some localised plasticity [1, 2], albeit at a smaller scale, and is the mechanism responsible for failure. After initiation for a critical stress state, the craze thickens by the growth of fibrils of which breakdown for a critical width results in the nucleation of a crack. In a numerical study [3] featuring a viscoplastic model for shear yielding and a viscoplastic cohesive zone for crazing, it was demonstrated that the competition between these two mechanisms together with the condition for the craze fibrils breakdown govern the level of the toughness, as for instance the ductile to brittle transition observed at low loading rates. A ductile response is related to the development of some plasticity in the bulk prior to crack propagation while a brittle response corresponds to the development of crazing only, the bulk remaining elastic. The present study is connected to a modelling of crazing [3, 4] within a cohesive surface methodology which incorporates the three stages of initiation, thickening and fibril breakdown of a craze. The purpose is to define a complete protocol to calibrate the parameters involved in this theoretical description. Since the condition for craze breakdown has been extensively investigated by interferometry with data available for instance in [5, 6], we borrow from these studies a condition based on a critical craze thickness for the nucleation of a crack. Therefore, the present study focuses on the characterisation of the first two stages of crazing: initiation and thickening. In order to illustrate the methodology, a calibration of the parameters used for the description of crazing in PMMA is presented.

1 COHESIVE ZONE FORMULATION FOR CRAZING

Experimental observations of crazes in glassy polymers typically show a craze thickness of some microns and a length of some decades larger. By neglecting the actual fibrillar microstructure of a craze, these two observations motivate the use of a cohesive surface to describe a craze [4]. Even if the physical mechanism for craze initiation is not clearly identified yet, various criteria are available in the literature which define a local critical stress σ^{cr} to be reached: a maximum principal stress is proposed in [7], the intermediate or the maximum shear stress in [8, 9] or a local critical deformation in [10]. All craze initiation formulations assume the side condition that $I_1 = \text{trace}(\underline{\sigma})$ is positive and that the craze plane is normal to the direction of maximum principal stress. Since there is no general agreement on which criterion has to be used, we will simply adopt the one that better fits our experimental results.

Once craze initiation takes place, the craze surfaces thicken by drawing material from a thin layer at the craze-bulk interface into the fibrils [1, 2]. This process is accompanied by an intense plastic deformation which is likely to be rate and temperature dependent for most polymers. Following Kramer's picture [1, 2] of craze thickening, Tijssens *et al.* [4] proposed a viscoplastic description for the opening within the framework of a cohesive surface as

$$\dot{\Delta}_n^c = \dot{\Delta}_0 \exp\left\{\frac{-A^c\sigma^c}{T}\left(1-\frac{\sigma_n}{\sigma^c}\right)\right\} \tag{1}$$

in which $\dot{\Delta}_n^c$ represents the craze thickening rate along the direction normal to the craze surface, σ_n is the normal traction with ($\dot{\Delta}_0$, A^c and σ^c) being material parameters. The pre exponential term $\dot{\Delta}_0$ characterises the time dependence, σ^c corresponds to an athermal stress for the craze thickening and A^c represents the temperature dependence. The craze fibrils thicken up to a critical value Δ_n^{cr} for which the fibrils break down which corresponds to the nucleation of a crack locally. The maximum thickness Δ_n^{cr} is also a material parameter which can fairly be taken constant in the case of PMMA, at a fixed temperature [5, 6].

Once the three stages of crazing are described, the cohesive surface formulation is completed with the traction-opening

$$\dot{\sigma}_n = k_n\left(\dot{\Delta}_n - \dot{\Delta}_n^c\right) \tag{2}$$

with n denoting the direction normal to the craze surfaces, $\dot{\Delta}_n$ the normal opening rate prescribed on a cohesive surface, $\dot{\Delta}_n^c$ the craze thickening rate (1) and k_n a stiffness. Prior to craze initiation, Equation (2) reduces to $\sigma_n = k_n\Delta_n$ in which the stiffness k_n has to be "infinitely" large to ensure that the elastic opening remains small and to prevent any discontinuity of the displacement field. Such a large stiffness also ensures that $\dot{\Delta}_n^c \approx \dot{\Delta}_n$ during thickening, which is consistent with Kramer's description [1, 2]. At the onset of craze fibrils breakdown, crack nucleation is represented by a vanishing normal stress σ_n for a displacement discontinuity Δ_n^{cr}. Note that for a linear elastic material subjected to a mode I loading, the energy release rate G_{IC} corresponds to the energy of separation for the creation of new surfaces as:

$$G_{IC} = \int_0^{\Delta_n^{cr}} \sigma_n\left(\dot{\Delta}_n^c\right) d\Delta_n. \tag{3}$$

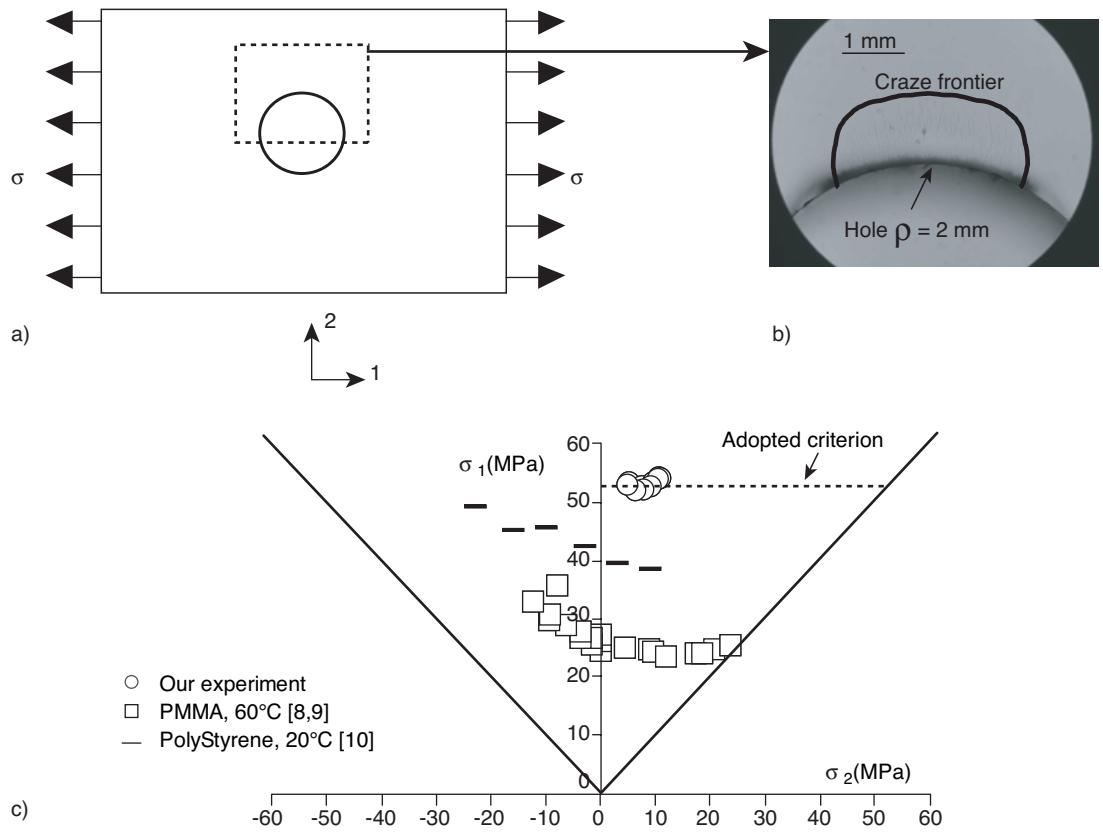

Figure 1

a) Schematic description of the device to analyse craze initiation; b) optical observation of the region with crazes; c) value of the stresses reported in the (σ_1, σ_2) principal stress space and comparison with data taken from the literature for PMMA at 60°C [8, 9] and for PolyStyrene [10]. The dashed line represents the adopted criterion based on a local maximum critical stress.

2 EXPERIMENTAL CALIBRATION

Commercial sheets of Polymethyl methacrylate (PMMA commercially called *Perspex*) of 10 mm thickness are used. The specimens employed for the analysis of craze initiation and craze thickening are extracted from the same plate. The measure of the molecular weight by size exclusion chromatography results in M_n= 864 kg/mol and M_w= 1843 kg/mol. Döll, and Döll and Könczöl [5, 6] observed and reported an influence of the molecular weight and related chain length on the development of a stable craze in amorphous polymers. For PMMA, a critical value of about M_n^{cr} = 200 kg/mol, below which no stable crazes are observed, is evidenced. For materials of which molecular weight M_n is larger than M_n^{cr}, Kramer's mechanism of crazing depicted in Section 1 operates. In our case and based on Döll's observations, the development of a stable craze is expected for the material under consideration. The principal and secondary relaxations were characterised by dynamic mechanical spectroscopy. The glass transition identified as the principal relaxation at 1 Hz is observed at 400 K while the β relaxation appears at 284 K, close to the room temperature.

2.1 Craze Initiation

The experimental configuration we use to investigate craze initiation is similar to that of Sternstein *et al.* [7] and consists in plate with a circular hole subjected to a remote constant tensile stress (see *Fig. 1a*). The crazes initiate at the equator of the hole and extend over a finite region. The observation of this region with an optical microscope shows a zone filled with crazes while the other is not *(Fig. 1b)*. The frontier between these two zones defines the local critical stress state for the craze initiation. The contour of the crazed region is observed to be stable for a loading time larger than twenty-thirty minutes and a

remote stress of 30 MPa. From the elastic solution of the problem and for various points regularly picked up along the craze frontier, we estimate the local principal stresses σ_1 and σ_2 which are reported in Figure 1c (circles). We observe that this contour corresponds to a drastic limitation in the stress space (σ_1, σ_2) since and $\sigma_1 = 55\,\text{MPa} \pm 2\,\text{MPa}$ and $\sigma_2 = 7\,\text{MPa} \pm 3\,\text{MPa}$ along the craze frontier. In Figure 1c, we reported the experimental data borrowed from [8, 9] and [10] for craze initiation and obtained respectively for PMMA at 60°C and PolyStyrene at room temperature. In the stress space $\sigma_1 > 0$ and $\sigma_2 > 0$, we observe that craze initiation takes place for a maximum principal stress approximately constant. Based on this observation and as a first approximation for the first stress quadrant ($\sigma_1 > 0$, $\sigma_2 > 0$), we adopt a craze initiation criterion based on maximum principal stress with $\sigma^{cr}_{1,\max} = 55\,\text{MPa}$ (supplemented with $I_1 > 0$), which is derived from our experimental measurements and represented by a dashed line in Figure 1c.

2.2 Craze Thickening

The aim of the present section is to identify the set of craze parameters ($\dot{\Delta}_0$, A^c and σ^c) involved in the description of the craze thickening rate (1). Since crazing is the mechanism responsible for failure and this process being assumed to be viscoplastic *(Equation 3)*, the material toughness is expected to be time dependent even if the bulk response is elastic. Therefore, the variation of the toughness with the loading rate is key for the calibration of the parameters used in the description of the craze thickening rate.

2.2.1 Experimental Procedure

Careful attention has been paid to the notching procedure as follows: a pre notch with a radius of 0.25 mm is machined by using a circular cutting wheel. In order to prevent heating while machining, specimens are cooled with compressed air. A sharp notch is further introduced at the tip of the pre notch by tapping a razor blade. The length of the crack is adjusted by using a falling weight system. This procedure is performed at room temperature and results in reproducible sharp cracks, with a length at least four times larger than the radius of the pre-notch, following the requirement of the ESIS-TC4 committee [11]. The observations of the sharp notches under crossed polarizers did not show any noticeable initial stress after this preparation. The samples are loaded under pure bending with a four points configuration to ensure mode I. In order to investigate the variation of the toughness with the loading rate, we prescribe a force rate ranging from 0.2 N/s to 200 N/s with an *Instron* servohydraulic tensile test machine. The loading rate is represented in terms of the rate of the stress intensity factor K_I. For a linear elastic material under pure bending, $K_I = \sigma_\infty \sqrt{\pi a} F(\alpha)$ with a the crack length, W the width of the specimen, $\alpha = a/W$ and the geometrical factor $F(\alpha) = 1.122 - 1.4\alpha + 7.33\alpha^2 - 13.08\alpha^3 + 14\alpha^4$ [12]. A constant value of $\dot{K}_I$ is prescribed through the force rate $\dot{F}$ and related stress rate $\dot{\sigma}$ remotely. The tests are performed at room temperature and atmosphere, for loading rates ranging from $\dot{K}_I = 10^{-3}\,\text{MPa}.\sqrt{\text{m}}/\text{s}$ to $\dot{K}_I = 1\,\text{MPa}.\sqrt{\text{m}}/\text{s}$. The load at fracture is used to derive the toughness K_{IC}, provided that the size requirements for plain strain and small scale yielding conditions

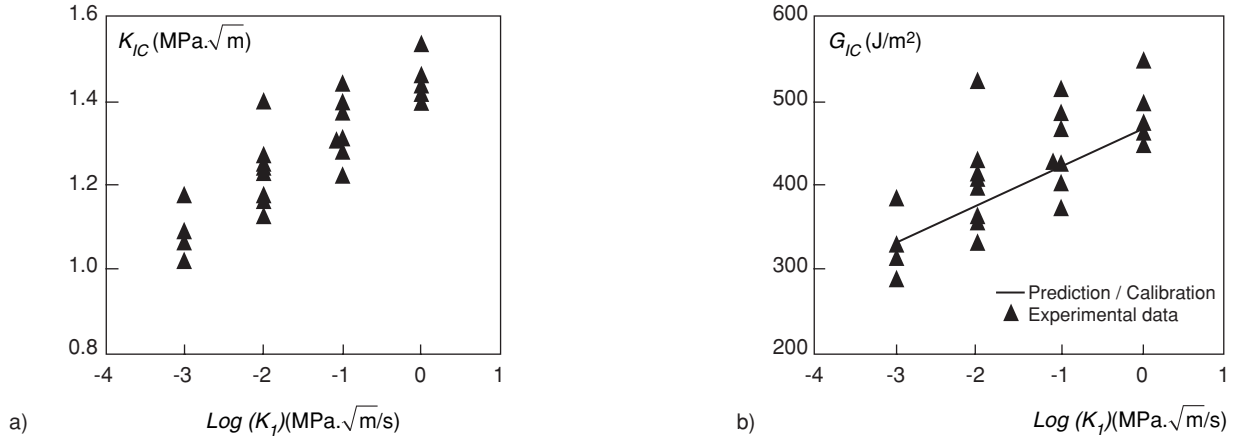

Figure 2

Variation of a) the critical stress intensity factor and b) the energy release rate with loading rate. PMMA with sharp notch, under mode I loading.

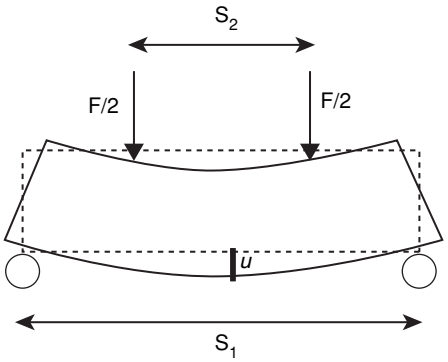

Figure 3

Schematic description of the four points bending configuration used with un-notched specimens loaded at various stress rates up to the remote stress corresponding to failure. The record of *F(u)* corresponding to fracture allows the estimate of the secant Young modulus representing the viscoelastic effects.

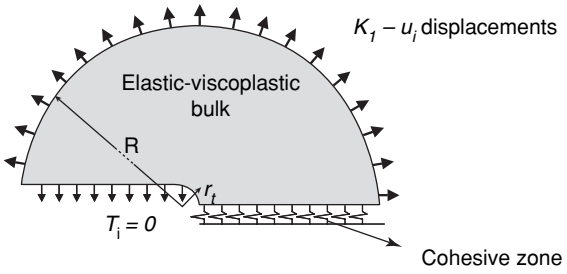

Figure 4

Problem formulation of the mode I small scale yielding configuration.

$$a, B, (W-a) \geq 2.5\left(\frac{K_{IC}}{\sigma_y}\right)^2, \qquad (4)$$

are fulfilled. The yield stress σ_y involved in (4) corresponds to that observed under tension at a loading rate such that the corresponding time scale $t_y = \sigma_y/\dot{\sigma}$ coincide with that of the fracture test $K_{IC}/\dot{K}_I$ [11]. Yielding is not observed in tension for PMMA since crazing and failure take place first under the loading conditions investigated here. The estimate of σ_y in (4) is obtained from the measure of the yield stress in uniaxial compression tests which is corrected by a factor 0.7 to account for its pressure sensitivity (ESIS-TC4 [11]). Following this method for the estimation of σ_y, a variation ranging from 66 MPa to 112 MPa is observed for loading rates ranging from $\dot{K}_I = 10^{-3}$ MPa.$\sqrt{\text{m}}$/s to $\dot{K}_I = 1$ MPa.$\sqrt{\text{m}}$/s. The size requirements (4) have been fulfilled for all fracture tests since the minimum length required is about one millimeter while the dimensions *a*, *W-a* an *B* are 10 mm.

2.2.2 Results

The variation of the toughness with loading rate is reported in Figure 2a. At the onset of crack propagation, unstable crack advance takes place and the related stress intensity factor corresponds to a critical K_{IC}. The observed increase of K_{IC} with loading rate $\dot{K}_I$ is not sufficient to conclude that failure is a time dependent process because of the viscoelastic effects, which need to be accounted for to estimate the energy release rate:

$$G_{IC} = K_{IC}^2 / E', \qquad (5)$$

with $E' = E/(1-\nu^2)$ for plane strain conditions, E the Young modulus and ν the Poisson ratio. The viscoelastic effects of the bulk are accounted for by measuring the secant modulus of an un-notched specimen loaded under identical conditions in terms of the remote stress rate $\dot{\sigma}$ (related to a prescribed $\dot{F}$). The measure of the displacement *u versus* the prescribed force *F* (see *Fig. 3*) is non linear and depends on the loading rate due to the viscoelastic effects. We propose to account for viscoelasticity by using the secant Young modulus corresponding to the measure of the displacement u^R and force F^R related to the remote stress σ^R for which failure is observed in the notched specimens. We then have the secant modulus:

$$E^{SECANT} = \frac{F^R}{u^R}\frac{1}{8BW^3}(S_1 - S_2)(2S_1^2 + 2S_1S_2 - S_2^2), \text{ with } S_1$$

and S_2 being the outer and inner span (see *Fig. 3*). The secant modulus is observed to vary from E = 3.22 GPa to E = 3.82 GPa for a force rate corresponding to $\dot{K}_I$ varying between 10^{-3} MPa.$\sqrt{\text{m}}$/s to 1 MPa.$\sqrt{\text{m}}$/s, showing that viscoelastic effects are not negligible. By accounting for this time dependence of the Young modulus and by assuming that the Poisson ratio is time independent, the variation of the energy release rate G_{IC} with the loading rate is reported in Figure 2b. We do observe an increase of G_{IC} with loading rate which evidences the viscous nature of the failure process.

3 CALIBRATION

The calibration is based on the comparison of the numerical predictions of the energy release rate with the experimental results reported in Figure 2b. The calculations are performed within a finite element analysis

Figure 5

Distribution of the plastic shear strain rate $\dot{\gamma}^P$: a) at craze initiation; b) prior to the onset of craze fibril breakdown; c) during crack propagation ($\dot{K}_I = 1\,\text{MPa.}\sqrt{\text{m}}/\text{s}$).

of mode I failure depicted in Figure 4 and detailed in [3]. Plasticity and crazing are assumed to be restricted around the crack tip so that the small scale yielding framework is allowed. The boundary layer approach is used to investigate the mode I plane strain conditions, as presented schematically in Figure 4. A cohesive surface is laid out along the crack symmetry plane, as observed experimentally. The remote region consists in a circular arc along which the K_I displacements fields are prescribed [3]. The constitutive law for the bulk material is elastic-viscoplastic and accounts for the specific softening upon yielding followed by progressive hardening as the deformation continues. The description of the bulk response is presented in [3, 13] to which the reader is referred for further details. Therefore, the bulk is not restricted to a linear elastic response but shear yielding and crazing are allowed as in [3].

In Figure 5, the distribution of the plastic shear strain rate $\dot{\gamma}^P$ is reported for a loading rate $\dot{K}_I = 1\,\text{MPa.}\sqrt{\text{m}}/\text{s}$ and the set of craze parameters ($\dot{\Delta}_0$, σ^c and A^c) to be presented in the next section. The variable $\dot{\gamma}^P$ is conveniently normalised by $\dot{\Gamma}_0 = \dot{K}_I \Big/ \left(s_0\sqrt{r_t}\right)$ which represents a prescribed shear strain rate at r_t (with the initial crack tip taken as r_t=5 µm), s_0= 216 MPa being the athermal yield stress of the bulk [3, 13]. In Figure 5, we have reported the plastic strain rate distribution (5a) at the onset of craze initiation, (5b) during craze thickening and prior to the craze fibril breakdown, (5c) during crack propagation. In this case, the bulk response shows negligible plasticity and is primarily elastic. In Figure 6, we reported the variation of the load level K_I (actually the normalised quantity $K_I/s_0\sqrt{r_t}$) *versus* the length of the craze *plus* crack. Once crazing initiates (circle in *Fig. 6*), craze growth results in a ductile response with an increasing load required for further craze thickening. At the onset of crack propagation (squares in *Fig. 6*), the crack advance takes place for a constant load level K_I, the value of which is used as K_{IC} for a given loading rate. The related energy release rate is derived from Equation (5) and compared to the experimental data. The simulations predict a craze length about 30 µm which is comparable to the measures reported in [5, 6]. By using the maximum principal stress $\sigma_1^{cr} = 55$ MPa for craze initiation and a critical thickness $\Delta_n^{cr} = 3$ µm for the condition of craze fibrils breakdown, the experimental data reported in Figure 2b are used to calibrate the parameters involved in the craze thickening rate ($\dot{\Delta}_0$, σ^c and A^c) in Equation (1). The identification of these three parameters requires more data than those presented and available in Figure 2b. In particular, the identification of the temperature dependence A^c needs additional experiments at various temperatures which have not been conducted here. As a first approximation, we assume an identical temperature dependence for

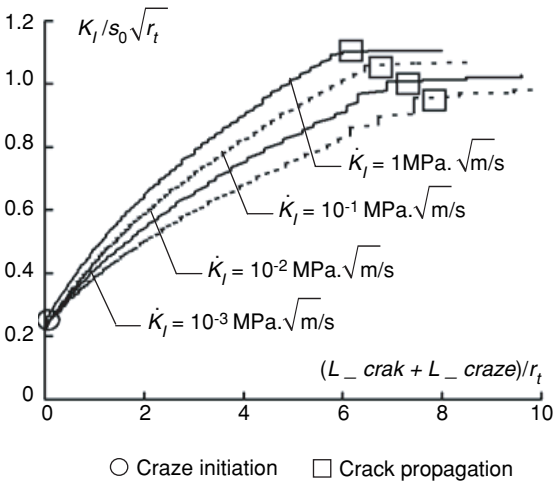

Figure 6

Influence of the loading rate on the resistance curves predicted for PMMA.

the craze thickening rate and for the bulk plastic deformation with A^c=60 K/MPa [14] as both processes involve some plasticity albeit at different scales. The two parameters (Δ_0, σ^c) are then adjusted to fit the experimental data presented in Figure 2b. Following a trial and error procedure, the pair (Δ_0, σ^c) which better captures the variations of G_{IC} with loading rate appears to be $(\Delta_0, \sigma^c) = (0.1\ \text{mm/s}, 140\ \text{MPa})$, the corresponding prediction being the curve in Figure 2b. We do observe that the model is able to capture the rate dependent toughness of glassy polymers.

CONCLUSION

An experimental protocol to calibrate the parameters of a viscoplastic cohesive zone that mimics crazing in glassy polymers is presented for PMMA. The model is able to capture the variation of the energy release rate with loading rate, of which rate dependency is evidenced experimentally. To capture this feature, a viscoplastic formulation for the cohesive zone is necessary. The parameters involved in the cohesive surface description have been identified and the experiments necessary to characterise craze initiation, craze thickening and craze fibril breakdown are presented. The present results need to be confirmed with some more comparisons in which, for instance, the stress triaxiality is varied. This will be the purpose of a forthcoming study.

REFERENCES

1 Kramer, E.J. (1983) Microscopic and molecular fundamentals of crazing. *Adv. Polym. Sci.*, **52-53**, 1-56.

2 Kramer, E.J. and Berger, L.L. (1990) Fundamental processes of craze growth and fracture. *Adv. Polym. Sci.*, **91-92**, 1-68.

3 Estevez, R., Tijssens, M.G.A. and Van Der Giessen, E. (2000) Modelling of the competition between shear yielding and crazing in glassy polymers. *J. Mech. Phys. Solids*, **48**, 2585-2617.

4 Tijssens, M.G.A., Van der Giessen, E. and Sluys, L.J. (2000) Modelling of crazing using a cohesive surface methodology. *Mech. Mater.*, **32**, 19-35.

5 Döll, W. (1983) Optical interference measurements and fracture mechanics analysis of crack tip craze zones. *Adv. Polym. Sci.*, **52-53**, 105-168.

6 Döll, W. and Könczöl, L. (1990) Micromechanics of fracture: optical interferometry of crack tip craze zone. *Adv. Polym. Sci.*, **91-92**, 138-214.

7 Sternstein, S.S., Ongchin, L. and Silverman, A. (1968) Inhomogeneous deformation and yielding of glasslike high polymers. *Appl. Polym. Symp.*, **7**, 175-199.

8 Sternstein, S.S. and Ongchin, L. (1969) Yield criteria for plastic deformation of glassy high polymers in general stress fields. *Polymer Prep. Am. Chem. Soc. Polymer Chem.*, **10**, 1117-1124.

9 Sternstein, S.S. and Myers, F.A. (1973) Yielding of glassy polymers in the second quadrant of principal stress space. *J. Macromol. Sci. Phys.*, **B8**, 539-571.

10 Oxborough, R.J. and Bowden, P.B. (1973) A general critical-strain criterion for crazing in amorphous glassy polymers. *Philos. Mag.*, **28**, 547-559.

11 Williams, J.G. and Pavan, A. (2001) *Fracture of Polymers, Composites and Adhesives II*, ESIS Publications.

12 Tada, H., Paris, P.C. and Irwin, G.R. (2000) *The stress Analysis of cracks Handbook*. Professional Engineering Publishing, London.

13 Wu, P.D. and Van der Giessen, E. (1996) Computational aspects of localized deformations in amorphous glassy polymers. *Eur. J. Mech. A-Solid.*, **15**, 799-823.

14 Saad-Gouider, N. (2005) Étude expérimentale et analyse numérique de la rupture des polymères amorphes, *Thesis*, INSA Lyon.

Final manuscript received in October 2006